

## Hydrothermal Synthesis of High Specific Capacity Al-doped $V_6O_{13}$ Cathode Material for Lithium-Ion Battery

Zhengguang Zou\*, Qi Yuan, Jilin Wang, Yao Gao, Yi Wu, Fei Long, Shichang Han, Zhendong Wan

College of Materials Science and Engineering, Guilin University of Technology, Guilin, China

\*E-mail: [zouzgglut@163.com](mailto:zouzgglut@163.com)

Received: 2 December 2016 / Accepted: 9 January 2017 / Published: 12 February 2017

Al-doped  $V_6O_{13}$  were synthesized via a facile hydrothermal method using vanadium pentoxide, oxalic acid dehydrate, aluminum nitrate nonahydrate and deionized water as the starting materials. XRD, FESEM, EDS and XPS were employed to characterize the phase, morphology, composition and valence of the as-synthesized samples. After doping  $Al^{3+}$ , the discharge specific capacity and cycle performance of the samples could be significantly improved. When the mole ratio of Al/V was 0.041, the sample exhibited the best electrochemical performance. The initial discharge specific capacity was  $496 \text{ mAh}\cdot\text{g}^{-1}$  and the capacity retention was 45.8% after cycling for 100 times. The enhanced electrochemical performance originated from that the sample was adhered together by stacking region in a regular arrangement and presented larger clearance between layers which could accommodate much more lithium-ion( $Li^+$ ) during the charge and discharge processes. Meanwhile, the increased specific capacity was attributed to the enhancement of the electrical conductivity after  $Al^{3+}$  doping.

**Keywords:** lithium-ion battery;  $V_6O_{13}$ ; Al-doped; electrochemical performance

### 1. INTRODUCTION

The specific capacity and cycle performance of lithium ion battery were depended on electrode materials capacity. Traditional cathode materials (such as  $LiCoO_2$ ,  $LiNiO_2$ ,  $LiMnO_2$  and  $LiFePO_4$ ) showed a low theoretical specific capacity, the specific capacity of these battery devices were about 150 mAh/g. Among various potential cathode candidates for lithium-ion battery, vanadium oxides had been extensively researched due to the multiple vanadium oxidation states, high specific capacity, widely availability and low cost. Multiple vanadium oxidation states (+2, +3, +4, +5) lead to single-valence and mix-valence vanadium oxides (for example  $VO_2$ ,  $V_6O_{13}$ ,  $V_3O_7$  and  $V_2O_5$ ). These compounds had partially filled d-orbitals indicating a particular electrochemical performance [1]. Compared to the other vanadium oxides,  $V_6O_{13}$  was one of the most promising candidate lithium-ion battery cathode materials because of the high theoretical specific capacity (420mAh/g) and electronic

conductivity [2-3].  $V_6O_{13}$  was composed of alternating single and double vanadium oxide layers.  $V^{4+}$  occupied the single and double layer sites of the V atoms and  $V^{5+}$  only occupied the double layer sites of V atoms [4]. Crystal structure of  $V_6O_{13}$  composed of  $VO_6$  octahedra, corner sharing single and double layers parallel to [010] plane [5]. The single and double layers alternate in the  $V_6O_{13}$  structure could provide much more sites for lithium intercalation [6, 7]. Theoretically,  $V_6O_{13}$  could electrochemically accommodate eight  $Li^+$  per formula unit, which could provide more  $Li^+$  during the process of lithium insertion and extraction [8]. Therefore,  $V_6O_{13}$  showed a high theoretical specific capacity and energy of 417 mAh/g and 900 Wh/kg, which were much higher than those of conventional  $LiMn_2O_4$  (148 mAh/g) [9, 10],  $LiCoO_2$  (274 mAh/g) [11] and  $LiFePO_4$  (170 mAh/g) [12]. In addition,  $V_6O_{13}$  had a high-rate charge and discharge due to its metallic character at room temperature.

The resistance of  $V_6O_{13}$  was closely related to its crystal lattice structures, which could significantly change in the lithium insertion and extraction process. After lithium inserting into  $V_6O_{13}$  structure, the formed  $Li_xV_6O_{13}$  would lead to the volume expansion and unstable structure [6, 7, 13]. So, the electronic conductivity of  $V_6O_{13}$  fell so quickly after lithium ion intercalation that the less utilization coefficient in high content lithium. Moreover, the large volume expansion/contraction and poor stability of crystal structures during lithium ion intercalation and deintercalation process may both interrupt the electronic and ionic contact pathways in the electrodes, leading to a rapid capacity fading [14]. Therefore, the way to improve the electrochemical performance of  $V_6O_{13}$  was not only reducing the internal resistance on the interface of electrolyte/ $V_6O_{13}$ , but also boosting the stability of crystal structure in the process of charge and discharge. S. N. Hua and M. Y. Saidi showed that  $V_6O_{13}$  coated with carbon was beneficial to obtain a high initial capacity (370 mAh/g), while the circulation property of battery was not obviously improve [15, 16]. The previous work had indicated that doping transition element could significantly enhance the electrochemical performance of  $V_6O_{13}$ . The synthesized  $Cr_{0.36}V_6O_{13.5}$  revealed good electrochemical performance with 370 mAh/g initial discharge capacity and capacity loss less than 15% after 35 cycles [17, 18].  $Mn_xV_{6-x}O_{13}$  ( $x=0.01, 0.02, 0.03, 0.04$ ) was synthesized via a hydrothermal method by Jinyun He, and they found that the sample doping with 2% Mn exhibited the best electrochemical performance (initial discharge capacity was 350.1 mAh/g and the capacity was restored to 282.7 mAh/g after 50 cycles) [19]. In our previous work,  $V_6O_{13}$  nanosheets were synthesized via hydrothermal method with  $V_2O_5$  and ethanol as reactant. However, the electrochemical performance cannot yet satisfactory, the initial discharge capacity was 330 mAh/g and the capacity retentions was 87% after 20 cycles [20].

On the one hand, aluminum was widely applied in semiconductor industry due to its low-cost, good conductive and environmental element in the earth crust. On the other hand, the radius of  $Al^{3+}$  (0.535 Å) was closed to that of  $V^{4+}$  (0.58 Å) and  $V^{5+}$  (0.54 Å). On the base of this, in our opinion,  $Al^{3+}$  was an appropriate dopant applied in  $V_6O_{13}$  cathode material for lithium-ion battery.

Herein, flower-like structure Al-doped  $V_6O_{13}$  were successfully synthesized via a hydrothermal reaction combined with the calcination process. The phase, morphology, composition and surface state of the samples were characterized through different testing methods. The series experiment of different doping contents what to study the influence of Al-doping on the morphologies, compositions and electrochemical performance of  $V_6O_{13}$ . On the basis of the obtained experiment results, the

possible influence mechanism of Al<sup>3+</sup> doping on the electrochemical performance was also discussed analyzed.

## 2. EXPERIMENTAL

All chemical reagents were analytical grade and used without any further purification. 1.25g oxalic acid dihydrate (C<sub>2</sub>H<sub>2</sub>O<sub>4</sub>•2H<sub>2</sub>O) and 0.4g vanadium pentoxide (V<sub>2</sub>O<sub>5</sub>) were dissolved in 20 mL of deionized water with stirring at 80 °C until a blue colored solution formed. The possible reaction was followed.



After cooled down to room temperature naturally, the mixture solution was filtered. A certain (Table 1) amount of aluminum nitrate nonahydrate (Al(NO<sub>3</sub>)<sub>3</sub>•9H<sub>2</sub>O) was dissolved in 15mL of deionized water and formed a transparent solution. Then this solution was added into as-obtained vanadyl oxalate(VOC<sub>2</sub>O<sub>4</sub>•5H<sub>2</sub>O) solution. And then 3 mL hydrogen peroxide 30%(H<sub>2</sub>O<sub>2</sub>) was added to above-mentioned mixed solution followed obtained a red transparent solution. The red mixed solution was transferred into a 100 mL stainless steel autoclave with continuous stirring until the bubbles disappeared. The autoclave was sealed and maintained at 160 °C for 24h. When the autoclave cooled down to room temperature naturally, the supernatant liquid was removed, the raw products were collected by centrifugation washed with deionized water, and dried in the freeze drier for 24 h. Finally, the obtained raw precursor was sintered at 350 °C for 1 h in argon in order to prepare Al-doped V<sub>6</sub>O<sub>13</sub>.

**Table 1.** Sample designations with doping different amount of Aluminum nitrate nonahydrate (Al(NO<sub>3</sub>)<sub>3</sub>•9H<sub>2</sub>O).

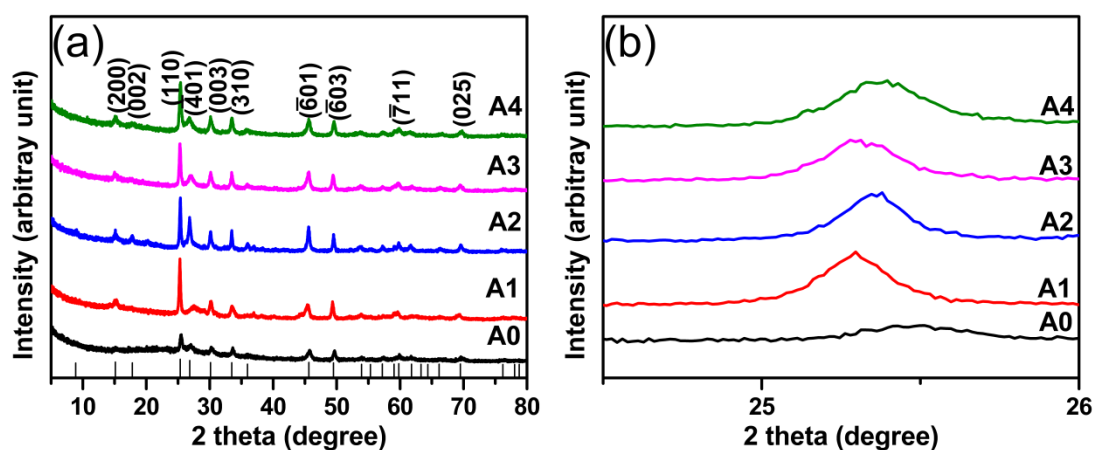
Sample designation	Al(NO <sub>3</sub> ) <sub>3</sub> •9H <sub>2</sub> O/g
A0	0.00
A1	0.02
A2	0.04
A3	0.06
A4	0.08

### 2.1. Characterization

The morphology were observed by Field emission scanning electron microscopy (FESEM, S-4800 Hitachi ). The phase were obtained by X-ray diffraction (XRD, X'Pert PRO MRD Panalytical). X-ray photoelectron spectroscopy (XPS, ESCALAB 250Xi Thermo Electron Corporation) analysis performed. Energy dispersive spectrometer (EDS, INCA IE 350 Oxford Instruments) was used to analyze component. The cycling performance were tested by NEWARE CT-3008 5V10mA-164 Battery Testing System (BTS). The properties and process of electrode reaction were measured by CHI 860D electrochemical workstation.

### 3. RESULTS AND DISCUSSION

Fig.1(a) illustrated the typical XRD patterns of Al-doped  $V_6O_{13}$ . For pure phase  $V_6O_{13}$ , there were main characteristic peaks at  $2\theta = 15.122, 17.803, 25.349, 26.842, 30.131, 33.487, 45.619, 49.496, 59.795$  and  $69.500$ , corresponding to (200), (002), (110), (003), (-401), (310), (-601), (-603), (-711) and (025) planes (JCPDS card No. 71-2235), respectively [21]. No other impurities were found. The diffraction peaks of Al-doped  $V_6O_{13}$  were also in good agreement with the standard diffraction peaks of pure phase  $V_6O_{13}$ . From the high angle diffraction pattern, the pattern peaks shifted to high angle after doping with  $Al^{3+}$  (figure 1(b)). It was because the ionic radius of  $Al^{3+}$  ( $0.535 \text{ \AA}$ ) was smaller than that of  $V^{4+}$  ( $0.58 \text{ \AA}$ ) and  $V^{5+}$  ( $0.54 \text{ \AA}$ ). The shift of the diffraction peaks indicated that  $Al^{3+}$  had incorporated into the lattice of  $V_6O_{13}$ .



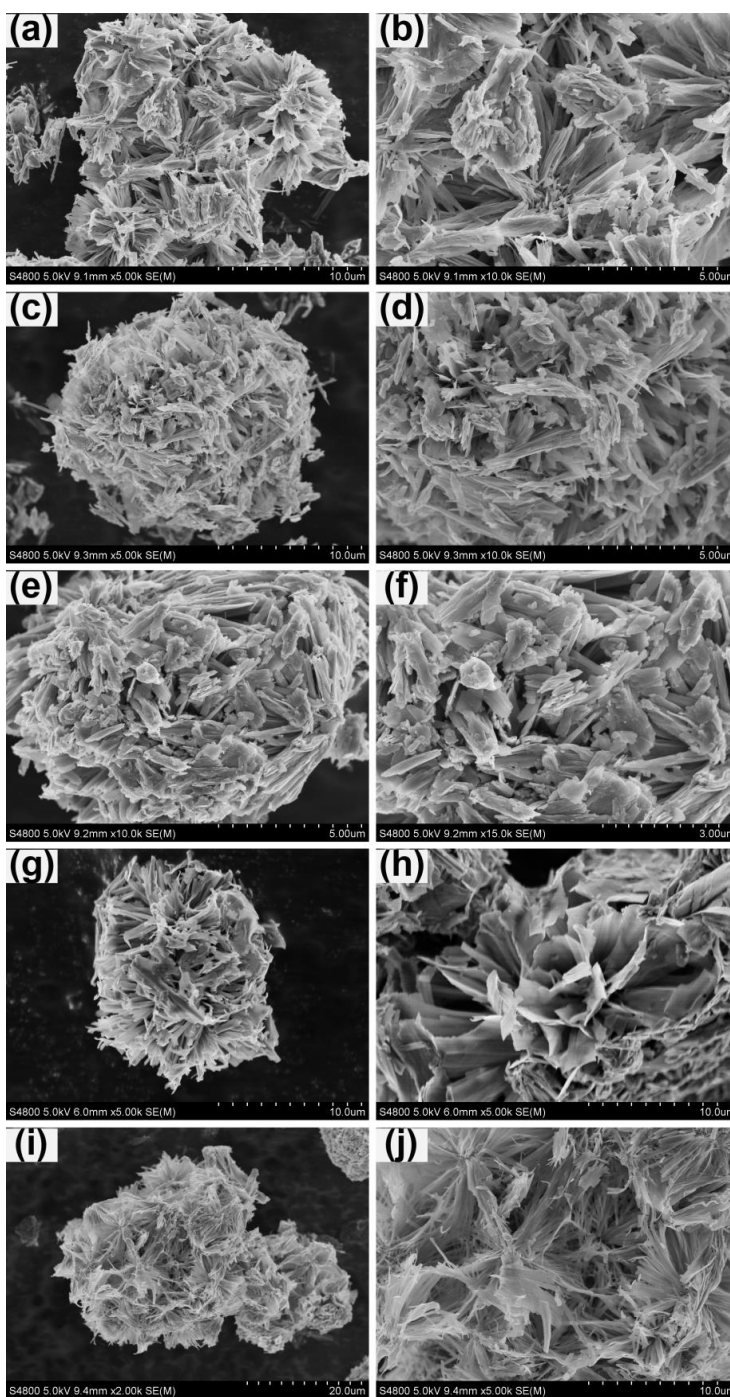
**Figure 1.** (a) The XRD patterns of A0, A1, A2, A3 and A4; (b) enlarged peaks at  $2\theta$  degree ranging from  $24^\circ$  to  $26^\circ$ .

Figure 2 showed the SEM images of Al-doped  $V_6O_{13}$  samples. The Al-doped  $V_6O_{13}$  revealed flower-like morphology which was assembled from lots of nanosheets (the thickness of less than 20 nm). The Al-doped  $V_6O_{13}$  samples of A0, A1 and A2 were slight agglomerated and adhered together by stacking region in an irregular arrangement with every unit, but A3 and A4 were adhered together by stacking region in a regular arrangement. Compared to the samples with low Al doping content (A1 and A2), the samples with high Al content (A3 and A4) had larger special surface area. These morphologies were beneficial to lithium transport in the charge and discharge process, leading to better electrochemical performance [22]. Besides, when the mole ratio of Al/V was 0.041, the sample (A3) presented larger clearance between layers. It could allow sufficient penetration of the electrolyte and effectively improve electrochemical performance of the lithium battery.

The compositions of as-obtained samples were tested by EDS. As showed in Table 2, as the content of aluminum increased, the Al/V (mass ratios and mole ratios) also increased. The EDS results indicated that aluminum had been doped in the structure of  $V_6O_{13}$  successfully.

**Table 2.** The mass ratio and mole ratio of aluminum to vanadium in different quantities Al-doped  $V_6O_{13}$ .

$Al(NO_3)_3 \cdot 9H_2O$	Al:V (mass ratio)	Al:V (mole ratio)
A1	0.006665:1	0.012589:1
A2	0.015071:1	0.028467:1
A3	0.021706:1	0.041000:1
A4	0.037212:1	0.070289:1

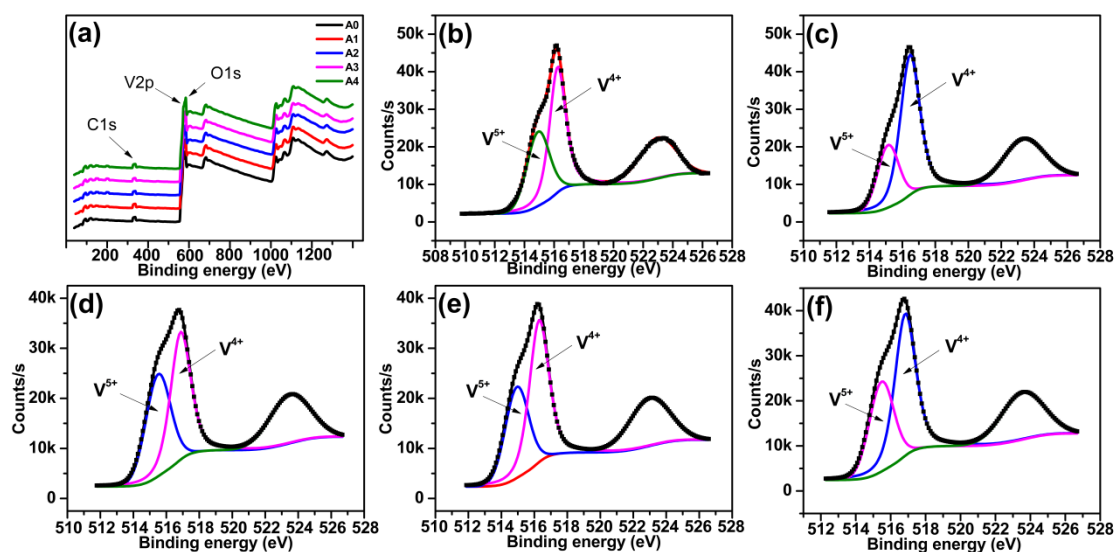


**Figure 2.** The typical SEM images of A0(a, b), A1(c, d), A2(e, f), A3(g, h) and A4(I, j) samples.

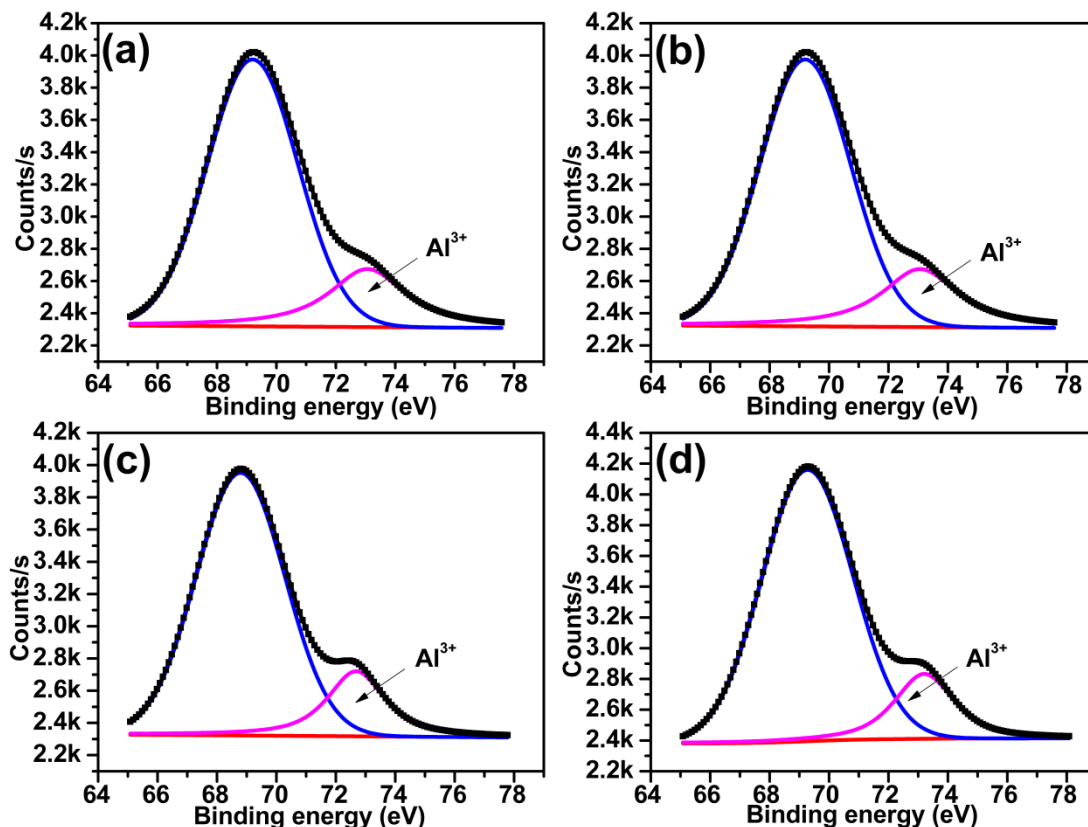
Fig. 3 (a) showed typical XPS spectra and their Gaussian-resolved components of O 1s, V 2p, N 1s and C 1s of Al-doped  $V_6O_{13}$ . Qualitative analysis of XPS spectra (Fig. 3a) demonstrated the presence of O, V, N and C. However, due to relatively low contents in the Al-doped  $V_6O_{13}$ , the corresponding peaks of Al was not obvious. The C elements may come from the reaction between  $VOC_2O_4$  and  $H_2O_2$ . The peak positions of +4 and +5 valences state of V 2p $_{3/2}$  core levels were slightly changed after Al doping (Fig. 3(b)-(f)). The peaks position of  $V^{5+}$  and  $V^{4+}$  were 515.10 and 516.28 eV (A0), 515.14 and 516.46 eV (A1), 515.50 and 516.86 eV (A2), 514.94 and 516.29 eV (A3), 515.47 and 516.29 eV (A4), respectively [22, 23]. The increment of binding energy suggested that Al could lead to a strong interaction between the vanadium and oxygen [24]. The ratio of  $V^{5+}$  and  $V^{4+}$  were 48.97% and 51.03% (A0), 29.47% and 70.53% (A1), 45.06% and 54.94% (A2), 39.20% and 60.80% (A3), 38.29% and 61.71% (A4), respectively. It was found that the  $V^{4+}$  hold the majority proportion and the ratio between  $V^{5+}$  and  $V^{4+}$  was close to that of the  $V_6O_{13}$  (1:2). However, after Al doped, the proportion of  $V^{4+}$  raised. It might be because the ionic radius of  $Al^{3+}$  (0.535 Å) was more close to  $V^{5+}$  (0.54 Å) than  $V^{4+}$  (0.58 Å), finally result in  $Al^{3+}$  replacing the site of  $V^{5+}$ .

Fig. 4 showed narrow-scan spectra in the Al 2p region and the resolved components for the Al-doped  $V_6O_{13}$  deposited at A1, A2, A3 and A4, respectively. The peak at 73.0 eV indicated that the oxidation state of Al was +3 [25-27].

The cyclic voltammetry curves of after three cycles for the Al-doped  $V_6O_{13}$  were characterized at a scan rate of  $0.1 \text{ mV}\cdot\text{s}^{-1}$  and a voltage scope of 1.5-3.5 V (Fig. 5). Four oxidation peaks occurred at around 2.35, 2.68, 2.84 and 3.31 V (versus  $Li^+/Li$ ) in A0, indicating Li ions intercalate into the non-equivalent sites in  $V_6O_{13}$ . Similarly, the reduction peaks located at around 2.04, 2.44, and 2.71 V (versus  $Li^+/Li$ ) were corresponded to the deintercalation of Li from the monoclinic  $V_6O_{13}$  [6, 8, 28, 29].



**Figure 3.** (a) XPS spectra and their Gaussian-resolved components of O 1s, V 2p, N 1s, C 1s and Si 2p. Narrow-scan spectra in the V 2p $_{3/2}$  region and the resolved components of A0(b), A1(c), A2(d), A3(e), A4(f).



**Figure 4.** Narrow-scan spectra in the Al 2p region and the resolved components of A1(a), A2(b), A3(c), A4(d).

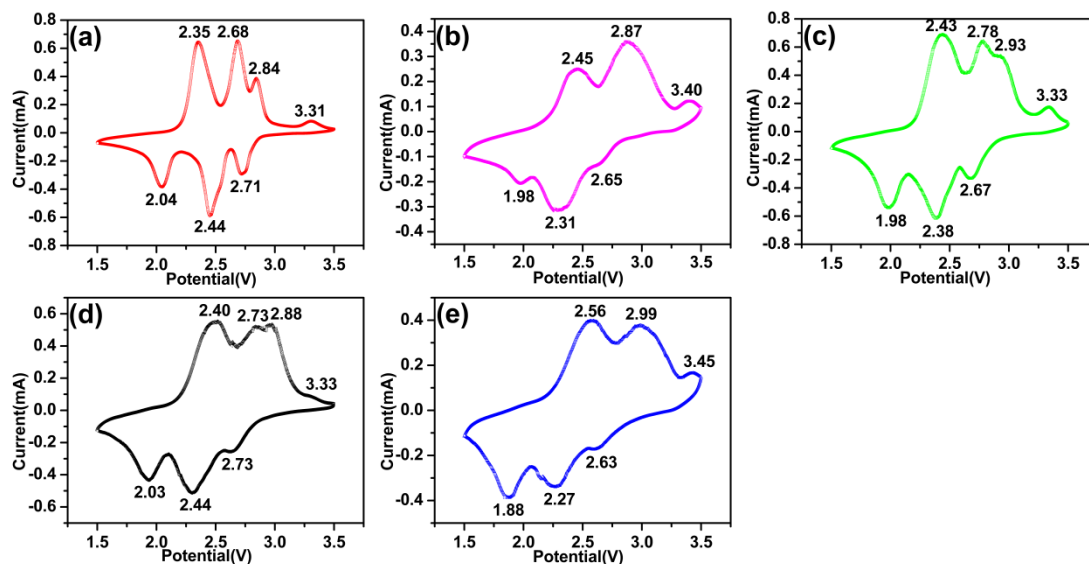


**Figure 5.** The cyclic voltammetry curves of the third cycle for A0(a), A1(b), A2(c), A3(d) and A4(e).

The structure of cyclic voltammetry curves was changed with increasing Al content in the system, the oxidation peaks centered at 2.45, 2.87 and 3.40 V (A1); 2.43, 2.78, 2.93 and 3.33 V (A2); 2.40, 2.73, 2.88 and 3.33 V (A3); 2.56, 2.99 and 3.45 V (A4). And the reduction peaks centered at 1.98, 2.31 and 2.65 V (A1); 1.98, 2.38 and 2.67 V (A2); 2.03, 2.44 and 2.73 V (A3); 1.88, 2.27 and

2.63 V (A4), respectively. It was found that with the increasing of doping content of Al, the oxidation peak first shift to lower voltage and then shift to higher (A3 was the smallest). Instead, the reduction peak first shift to higher voltage then shift to lower (A3 was the largest). The cyclic voltammetry curves of A3 were shown the largest polarization.

The cycling performance of Al-doped  $V_6O_{13}$  was further investigated in Figure 6(a). The reversible discharge capacity can be obtained at a rate of  $42 \text{ mA}\cdot\text{g}^{-1}$  in 1.5-4.0 V. The initial discharge capacity of Al-doped  $V_6O_{13}$  were  $241 \text{ mAh}\cdot\text{g}^{-1}$  (A0),  $289 \text{ mAh}\cdot\text{g}^{-1}$  (A1),  $330 \text{ mAh}\cdot\text{g}^{-1}$  (A2),  $496 \text{ mAh}\cdot\text{g}^{-1}$  (A3) and  $355 \text{ mAh}\cdot\text{g}^{-1}$  (A4), respectively. The capacity could be enhanced after doping Al into  $V_6O_{13}$  crystal lattice, it was because that good electrical conductivity Al element doping into  $V_6O_{13}$  samples [26]. With the Al doping content increasing, the initial discharge capacity of the Al-doped  $V_6O_{13}$  increased at first and then descended. When the mole ratio of Al/V was 0.041, the initial discharge capacity was the highest. The discharge capacity of A3 was also high than  $450 \text{ mAh}\cdot\text{g}^{-1}$  after 30 cycles. The capacity retentions of Al-doped  $V_6O_{13}$  were 32.0% (A0), 47.1% (A1), 27.0% (A2), 45.8% (A3) and 17.5% (A4) after 100 cycles, respectively. It was noted that the the capacity declined sharply when the mole ratio of Al/V was 0.070 (A4). It was because high content of Al could destroy  $V_6O_{13}$  crystal structure followed caused low capacity retention [21, 30]. The result showed that the electrochemical performance of Al-doped  $V_6O_{13}$  was much better than the other cathode materials [15-20], as showed in Table 3.

**Table 3.** The electrochemical performance of Al-doped  $V_6O_{13}$  and the other cathode materials.

cathode material	initial discharge capacity ( $\text{mAh}\cdot\text{g}^{-1}$ )	capacity retention (%) / cycle number
$V_6O_{13}$	330	87/20
$V_6O_{13}$ coated with carbon	370	-
$\text{Cr}_{0.36}\text{V}_6\text{O}_{13.5}$	370	85/35
$\text{Mn}_x\text{V}_{6-x}\text{O}_{13}$	350	81/50
Al-doped $V_6O_{13}$	496	91/30

Fig. 6 (b)-(f) showed the first, fiftieth and hundredth charge–discharge curves of the samples A0, A1, A2, A3 and A4 at current densities of  $42 \text{ mA}\cdot\text{g}^{-1}$ , respectively. All the charge-discharge curves had three obvious discharging platforms, indicating that the cathode material carried on a phase transition process after lithium ion intercalation. The three discharging platforms located at near 2.0 V, 2.3 V and 2.7 V. This suggested that the Al element doping could effectively obtain stable V-O species and suppress the electrolyte degradation [31].

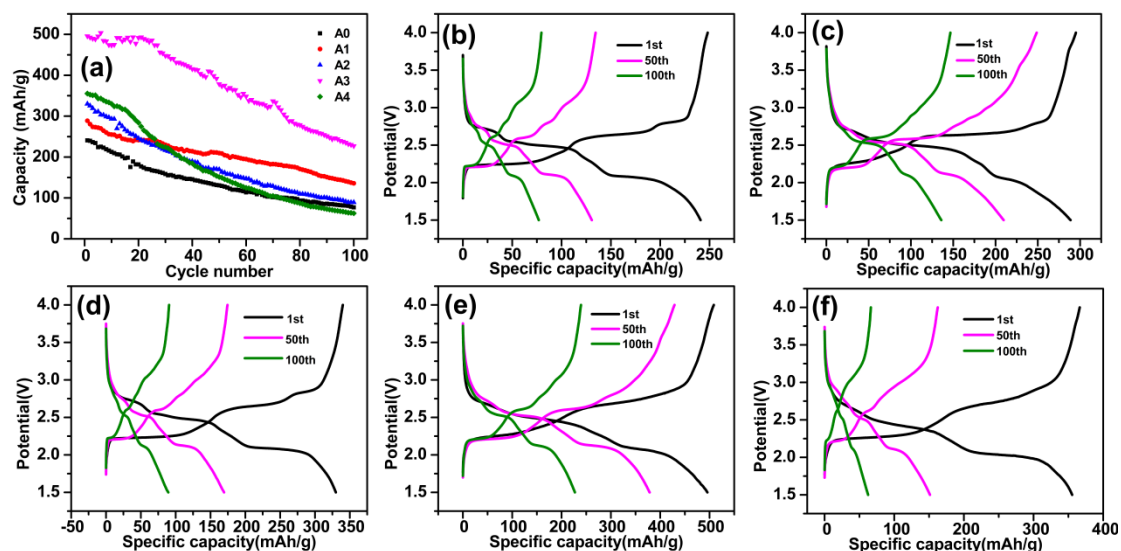


**Figure 6.** (a) Cycling performance of A0, A1, A2, A3 and A4 electrodes at 0.1 C; The first, fiftieth and hundredth charge-discharge curves of A0(b), A1(c), A2(d), A3(e) and A4(f) at current densities of  $42 \text{ mA}\cdot\text{g}^{-1}$  in the voltage range of 1.5-4.0 V.

#### 4. CONCLUSION

Al-doped  $\text{V}_6\text{O}_{13}$  were synthesized via a facile hydrothermal method. The Al-doped  $\text{V}_6\text{O}_{13}$  revealed flower-like morphology which was adhered together by stacking region with every unit. A0, A1 and A2 were slight agglomerated and adhered together by stacking region in an irregular arrangement, but A3 and A4 were adhered together by stacking region in a regular arrangement. The electrochemical tests showed that the discharge specific capacity and cycle performance of the samples could be significantly improved after doping  $\text{Al}^{3+}$ . When the mole ratio of Al/V was 0.041, the sample exhibited the best electrochemical performance. The initial discharge specific capacity was  $496 \text{ mAh}\cdot\text{g}^{-1}$  and the capacity retention was 45.8% after cycling for 100 times. The enhanced electrochemical performance originated from larger clearance between layers that allow sufficient penetration of the electrolyte. These morphologies were beneficial to lithium transport in the charge and discharge process. Meanwhile, the increased specific capacity was attributed to the enhancement of the electrical conductivity after  $\text{Al}^{3+}$  doping.

#### ACKNOWLEDGEMENT

This work was supported by the National Nature Science Foundation of China (Project No. 51562006) and Improving the Basic Ability of Young and Middle-aged University Teachers in Guangxi (No. KY2016YB187).

#### References

1. J. Haber, M. Witko and R. Tokarz, *Appl Catal A-Gen*, 157 (1997) 3.
2. N. Peys, Y. Ling, D. Dewulf, S. Gielis, C. D. Dobbelaere, D. Cuypers, P. Adriaensens, S. V. Doorslaer, S. D. Gendt, A. Hardy and M. K. V. Bael, *Dalton Trans*, 42 (2013) 959.

3. Y. Y. Xia, T. Fujieda, K. Tatsumi, P. P. Prosini and T. Saka, *J Power Sources*, 92 (2001) 234.
4. D. W. Murphy, P. A. Christian, F. J. Disalo and J. Lithium, *Inorg Chem*, 18 (1979) 2800.
5. D. Murphy, P. Christian, F. DiSalvo, J. Carides and J. Waszczak, *J Electrochem Soc*, 128 (1982) 2053.
6. H. Björk, S. Lidin, T. Gustafsson and J. O. Thomas, *Acta Crystallogr B*, 57 (2001) 759.
7. J. Höwing, T. Gustafsson and J. O. Thomas, *Acta Crystallogr B*, 59 (2003) 747.
8. K. West, B. Zachau-Christiansen, T. Jacobsen and S. Atlung, *J Power Sources*, 14 (1985) 235.
9. L. W. Liu, W. Tian and X. Q. Zhao, *Chinese Battery Industry*, 8 (2003) 147.
10. X. Shi, W. H. Pu and Y. L. Wu, *Chemical Industry and Engineering Progress*, 30 (2011) 1264.
11. D. Huang, *Advanced Battery Technology*, 11 (1998) 23.
12. X. Dai, H. H. Tang and P. Yang, *Materials Review*, 19 (2006) 69.
13. J. Barker, E. S. Saidi and M. Y. Saudi, *Electrochim Acta*, 40 (1995) 949.
14. J. Barker, R. Koksang, *Electrochim Acta*, 40 (1995) 673.
15. S. N. Hua, S. Phang, *J Power Sources*, 10 (1983) 279.
16. M. Y. Saidi, J. Barker, *Solid State Ionics*, 78 (1995) 169.
17. P. Soudan, J. P. Pereira-Ramos, J. Farcy, G. Gregoire and N. Baffier, *Solid State Ionics*, 135 (2000) 291.
18. C. Leger, S. Bach, J. P. Pereira-Ramos, *J Solid State Electr*, 11 (2007) 71.
19. J. Y. He, F. Long, Z. G. Zou, *Ionics*, 21 (2015) 995.
20. Z. G. Zou, H. Chen, J. Y. He, F. Long, Y. Wu, Z. Y. Yan, H. X. Chen. *Electrochimica Acta*, 135 (2014) 175.
21. S. Y. Zhan, C. Z. Wang, K. Nikolowski, H. Ehrenberg, G. Chen, Y. J. Wei, *Solid State Ionics*, 180 (2009) 1198.
22. C. Nethravathi, C. R. Rajamathi, M. Rajamathi, U. K. Gautam, X. Wang, D. Golberg, Y. Bando, *ACS Applied Materials & Interfaces*, 5 (2013) 2708.
23. Q. Shi, W. Huang, Y. Zhang, J. Yan, Y. Zhang, M. Mao, Y. Zhang and M. Tu, *ACS Applied Materials & Interfaces*, 3 (2011) 3523.
24. X. F. Wu, Z. M. Wu, C. H. Ji and H. F. Zhang, *Applied Materials & Interfaces*, 8 (2016) 11842.
25. M. Chen, X. Wang, Y. H. Yu, Z. L. Pei, X. D. Bai and C. Sun, *Appl Surf Sci*, 158 (2000) 134.
26. J. P. Kar, S. Kim, B. Shin, K. I. Park, K. J. Ahn, W. Lee, J. H. Cho and J. M. Myoung, *Solid State Electron*, 54 (2010) 1447.
27. K. Uma, M. Rusop, T. Soga and T. Jimbo, *J Appl Phys*, 46 (2007) 40.
28. M. Simoes, Y. Surace, S. Yoon, C. Battaglia, S. Pokrant and A. Weidenkaff, *J Power Sources*, 291 (2015) 66.
29. O. Bergstroem, T. Gustafsson and J. O. Thomas, *Solid State Ionics*, 110 (1998) 179.
30. J. Howing, T. Gustafsson and J. O. Thomas, *Acta Crystallogr B*, 1 (2004) 382.
31. M. S. Whittingham, *Chem Rev*, 1 (2004) 4271.